Advanced Composites and Hybrid Materials (2025) 8:281
https://doi.org/10.1007/s42114-025-01358-2

RESEARCH

Giant, non-perturbative tuning of light-matter interaction of embedded quantum dots in semiconducting matrices

Ming-Chung Wu[1,2,3,4] · Kai-Chi Hsiao[1] · Chuliang Fu[5] · Ting-Han Lin[1,2] · Yin-Hsuan Chang[1] · Yu-Ching Huang[1,2,4] · Mu-Ping Nieh[6] · Wei-Fang Su[4,7] · Mingda Li[5]

Received: 29 June 2024 / Revised: 5 May 2025 / Accepted: 5 June 2025
© The Author(s) 2025

Abstract
Embedding quantum dots (QDs) in a solid-state matrix represents a promising hybrid platform that offers great flexibility and tunability. However, the lack of clear underlying designing principle and presence of large design space make the design process heavily relies on trial-and-error methods. Here we present a new principle that can drastically tailor the light-matter interaction of matrix by matrix-mediated QD interactions. We show that conducting matrices like P3HT can mediate a non-perturbative inter-QD interactions that lead to qualitatively distinct properties, including the enhanced carrier lifetime and enhanced binding energies with increased QD densities, which cannot be explained by conventional perturbative scattering theories and in sharp contrast to independent embedded QDs in an insulating matrix like PMMA. An effective quantum-field-theory is developed, showing qualitative agreement with experiments. Our study serves as a foundation for the predictive design of advanced hybrid materials aimed at optimizing functionalities.

Keywords Perovskite quantum dots · Semiconducting matrices · Insulator matrix · Quantum-field-theory

1 Introduction

Hybrid materials composed of 3D defects, such as quantum dots (QDs) and nanoparticles, embedded in a solid matrix material, have garnered widespread interest due to their distinctive properties and potential applications in various fields. Such 3D defects in solids can be used to tailor electrical and optical [1–11], magnetic [12–19], and thermal properties [20–24], with huge potential benefits for applications such as solar energy harvesting [1–4, 25–28], battery [29], sensing [30–35], and thermoelectrics [36, 37]. As breakthroughs in material science continue to drive technological revolutions, the exploration of such hybrid structures opens new frontiers for next-generation functional materials. With large tunability and great versatility, the 3D defect-solid matrix structure presents a new class of hybrid materials with novel material phases and superior performance, far beyond what is achievable through chemical doping [38]. QDs, in particular, exhibit exceptional luminescent properties, including narrow emission bandwidths, adjustable emission wavelengths, and high photoluminescent quantum yields (PLQY). Recent studies emphasize the crucial role of the matrix in modulating the optical properties of QDs. For instance, the type of matrix significantly influences the

✉ Ming-Chung Wu
mingchungwu@cgu.edu.tw

✉ Mingda Li
mingda@mit.edu

1 Department of Chemical and Materials Engineering, College of Engineering, Chang Gung University, Taoyuan 333323, Taiwan

2 Center for Sustainability and Energy Technologies, Chang Gung University, Taoyuan 333323, Taiwan

3 Division of Neonatology, Department of Pediatrics, Chang Gung Memorial Hospital at Linkou, Taoyuan 333423, Taiwan

4 Department of Materials Engineering, Ming Chi University of Technology, New Taipei City 243303, Taiwan

5 Department of Nuclear Science and Engineering, Massachusetts Institute of Technology, Cambridge, MA 02139, USA

6 Department of Chemical and Biomolecular Engineering, University of Connecticut, Storrs, CT 06269, USA

7 Department of Materials Science and Engineering, National Taiwan University, Taipei City 106319, Taiwan

Published online: 21 June 2025

photoluminescence (PL) emission intensity and lifetime of embedded QDs. Surface passivation and defect mitigation through matrix interactions are pivotal for enhancing light-matter coupling [39–41]. These findings highlight the importance of designing matrix-mediated QD interactions to tailor light-matter interactions, offering new opportunities in hybrid material design. This emerging paradigm underscores the transformative potential of 3D defect-solid matrix structures in advancing material science.

Semiconductor nanocrystals are typically synthesized through the bottom-up routes such as hot-injection and supersaturated recrystallization or top-down method of the ball-milling method [42] or liquid-phase exfoliation [43]. Both top-down and bottom-up syntheses aim to reduce the sizes of materials. The continuous energy level of bulk materials becomes discrete after their sizes reduce to nanometer scale. When confining the size of a semiconductor at a nanoscale level, the continuous energy level of bulk materials becomes discrete. The quantum confinement effect results in an increased energy bandgap. The quantum confinement effect is induced as the size of nanocrystals is smaller than their Bohr excitonic radius [44, 45]. Different from other types of quantum dots, namely the IV, III–V, II–VI, IV–VI, I–III, and VI_2 family, the energy level of perovskite quantum dots (PQDs) can be manipulated not only by their size but also by their chemical composition. That allows another degree of freedom for PQDs to tune their energy bandgap and cover the entire visible band. Inheriting from bulk perovskite, the PQDs exhibit "high defect tolerance" [46]. It implies the intrinsic defects in PQDs do not serve as electron or hole annihilation sites, and it confers PQDs to perform near-unity photoluminescence quantum yield (PLQY) [47, 48]. Regarding QD-semiconductor matrices, colloidal PbS QD has been implemented into perovskite to construct a quantum dot-in-perovskite solid [27]. The QD in such a system plays not only an epitaxial site for crystallization but also a carrier collection site that prolong the carrier lifetime. In addition to carrier transfer property, an evolution of thermoelectric property of QD-semiconductor matrix has also been reported. Conductive polymer of PEDOT can achieve an outstanding thermoelectric property with power factor of 63.1 $\mu W/mK^2$, being the highest record for PEDOT-metal composite, with assistance of silver quantum dot embedding [49]. Yet, the beneath mechanism of how QDs interact with the embedding matrix is still unclear and lacks solid principle toward performance optimization.

To realize a new functional material, simulations such as density-functional theory are often implemented. However, in the case of QD-matrix hybrid, the involvement of at least tens of thousands of atoms leads to an unbearably high computational cost, posing a significant challenge in guiding the materials design. A few semi-empirical models have been established to deal with the interaction of 3D defects with internal structures. Coulomb-scattering [50–54], Mayadas-Shazkes model [55, 56], and hard-sphere model have been established for revealing the interaction about one-dimensional dislocation, two-dimensional grain boundaries, and nanoparticle scattering [57]. Although some quantities can be extracted, these models share severe limitations. The predictions based on the *pre-assigned* physical process that is destined to happen are difficult to frame and are close to the reality of the entire system from these models. Also, the first-order theories and single-particle models can not reveal the many-body correlation and higher-order scattering. That is the Achilles' heel for semi-empirical models because the correlation effect associated with the internal excitations is a key to many exotic phenomena, such as the Kondo effect [58] or the Coulomb blockade [59]. These high order effects are the trigger for driving the system toward qualitative changes that confer another degree of freedom to tune the physical properties.

In this work, we aim to study the effect of 3D QD defects with internal structure and random spatial distribution to the properties to the solid-state matrix. We demonstrate two systems for quantum dots embedded matrices to discuss the light-matter interaction differences between $CsPbBr_3$ QD-embedded P3HT (quantum dot-in-semiconductor matrix, QD-P3HT matrix) and $CsPbBr_3$ QD-embedded PMMA (quantum dot-in-insulator matrix, QD-PMMA matrix) as a reference. Surprisingly, the QD-P3HT with conducting matrix shows a number of unexpected phenomena and QD density dependence in terms of carrier lifetime and binding energy. The phenomena of how the exotic impurities tailor the relaxation time and self-energy of electron–hole pairs are described by an effective quantum field theory, showing a non-perturbative nature. That perfectly matches with experimental observation and offers a clear guideline for exotic 3D QD defects to other degrees of freedom for giant property tuning.

2 Experimental section

2.1 Synthesis of $CsPbBr_3$QD

To synthesize $CsPbBr_3$ quantum dots (QDs), Cs-oleate precursors were first prepared. Specifically, 2.5 mmol Cs_2CO_3 (0.814 g, 99.5%, Acros) was transferred into a three-necked flask along with 40 mL of octadecene ($C_{18}H_{36}$, 90%, Thermo) and 2.5 mL of oleic acid ($C_{18}H_{34}O_2$, 90%, Sigma-Aldrich). The reactants were degassed at 120 °C for 1 h. After degassing, the reactor was maintained at 150 °C until all the Cs_2CO_3 was capped with oleic acid and dispersed in the solvent. For the synthesis of $CsPbBr_3$ QDs, 0.087 g of $PbBr_2$ (98 + %, Alfa Aesar) was transferred into another three-necked flask with 0.5 mL of n-oleylamine ($C_{18}H_{37}N$, C18-content 80–90%,

Acros), 0.5 mL of oleic acid, and 5 mL of octadecene, and the mixture was heat-treated at 120 °C for 1 h under vacuum. Subsequently, the temperature was increased to 150 °C to dissolve the $PbBr_2$ into the solution. 0.4 mL of the hot Cs-oleate solution was swiftly injected, and the reactor was immediately placed into an ice bath to quench the temperature to room temperature. Finally, 10 mL of methyl acetate ($C_3H_6O_2$, 99%, Acors) was added to precipitate the product, which was then collected by centrifugation. To be compatible with polymers of P3HT (M.W. ~ 60,000 Da) and PMMA (M.W. ~ 120,000 Da, Sigma-Aldrich), the collection was further redispersed into anhydrous chlorobenzene with concentration about 30 wt.%.

2.2 Preparation of $CsPbBr_3$/PMMA or P3HT

A desired concentration of 1 wt.% of P3HT or PMMA were prepared by 100 mg of polymer dissolved into 9900 mg of anhydrous chlorobenzene (C_6H_5Cl, > 99%, ACROS) into a 20-mL vial bottle, respectively as pristine polymer solutions. For $CsPbBr_3$ quantum dot mixed polymer solutions, concentrated solution of 10 wt.% to polymer solute was prepared first and noted as 10.0 wt.% QD in polymers. To obtain the desired concentration of QD in polymers, the concentrated QD in polymer solution were mixed with pristine polymer solution and obtain the desired precursor solution from 1.0 wt% QD to 5.0 wt% QD in PMMA or P3HT.

2.3 Characterization

Microstructure was observed via a spherical-aberration corrected field emission transmission electron microscope (JEOL JEM-ARM200FTH). The optical characteristics are explored through photoluminescence spectroscopy with a 405-nm and 532-nm diode laser (LDH-PC-375, PicoQuant). The temperature-dependent PL spectra were carried out in a well-confined chamber with a quartz observation window. The PL spectra of quantum dots embedded either PMMA or P3HT were characterized with a 405-nm diode laser. On the other hand, the PL spectra of P3HT matrices were examined by a 532-nm diode laser. The temperature varied from room temperature of 303 to 103 K being the limitation of in-house liquid-N_2 cooling system and the spectra were collected every 20 K. The binding energy of both quantum dot and P3HT were all extracted from the integrated emission intensity of PL spectra. The information about binding energy can be revealed based on Arrhenius's equation.

3 Result and discussion

3.1 Characteristics of QDs

QDs have emerged as key components due to their unique optical and electronic properties. Among various types, cesium lead tribromide ($CsPbBr_3$) QDs have earned significant attention for their potential applications in light-emitting devices, solar cells, and photodetectors. The hot-injected $CsPbBr_3$ QD showed well-dispersity in the non-polar solvent of toluene or chlorobenzene. Owing to the adsorbed ligand at the ending facet of QD, the shape and size of QD can be effectively controlled by the assistance of the applied ligand. Ligand-mediated nanocrystal synthesis has been reported as a feasible strategy to tune the shape and size of nanoparticles. The reduced surface energy for a certain facet of ligand-adsorbed nanoparticles makes nanoparticles tend to grow in a certain shape. As shown in Fig. 1a, the QD synthesized with the assistance of long alky chain ligands of oleylamine and oleic acid tended to grow in a cubic shape. HR-TEM of the QD was shown in Fig. 1b. The particle size distribution (Fig. 1c) further quantifies this information, offering statistical insight into the uniformity and control achieved during the synthesis process. The clear lattice was indicative of the preferred orientation in (200) and high crystallinity of QD. The calculated *d* spacing was 2.93 Å, which is referred to as the plane (200) of QD. After optimizing the reaction duration (5 s) and temperature (150 °C), the particle size was homogenously distributed with an average size of 5.80 nm as shown in Fig. 1c. The high-resolution TEM image (Fig. 1d) provides the crystalline lattice of the QDs, showcasing their well-defined structure. This level of detail is crucial for understanding the quantum confinement effect that governs the optical properties of QDs. Complementing this, the diffraction patterns (Fig. 1e) confirm the crystalline phase and purity of the $CsPbBr_3$ QDs, serving as a fingerprint of their structural integrity. The specific area in HR-TEM was selected for *d* spacing calculation and the corresponding depth profile was shown in Fig. 1f. This analysis reveals the periodicity and spatial distribution of atoms within the QDs, providing deeper insights into their crystal structure. Figure 1 g shows the crystal structure of $CsPbBr_3$. The detailed examination of the crystal structure of $CsPbBr_3$ lays the foundation for understanding the relationship between structure and optical properties. The optical characteristics of $CsPbBr_3$ QDs are further explored through photoluminescence (PL) spectra (Fig. 1h). The PL spectra offer a glimpse into the electronic band structure and the recombination processes of charge carriers within the QDs. Accompanying the spectra, photos of various QD solutions under UV light demonstrate the tunability of their emission colors, a property that is highly desirable for optoelectronic applications (Fig. 1i). In conclusion, the comprehensive analysis of $CsPbBr_3$ QDs through TEM imaging, particle size distribution, diffraction patterns, and PL spectroscopy reveals the intricate details of their structural and optical properties. These insights

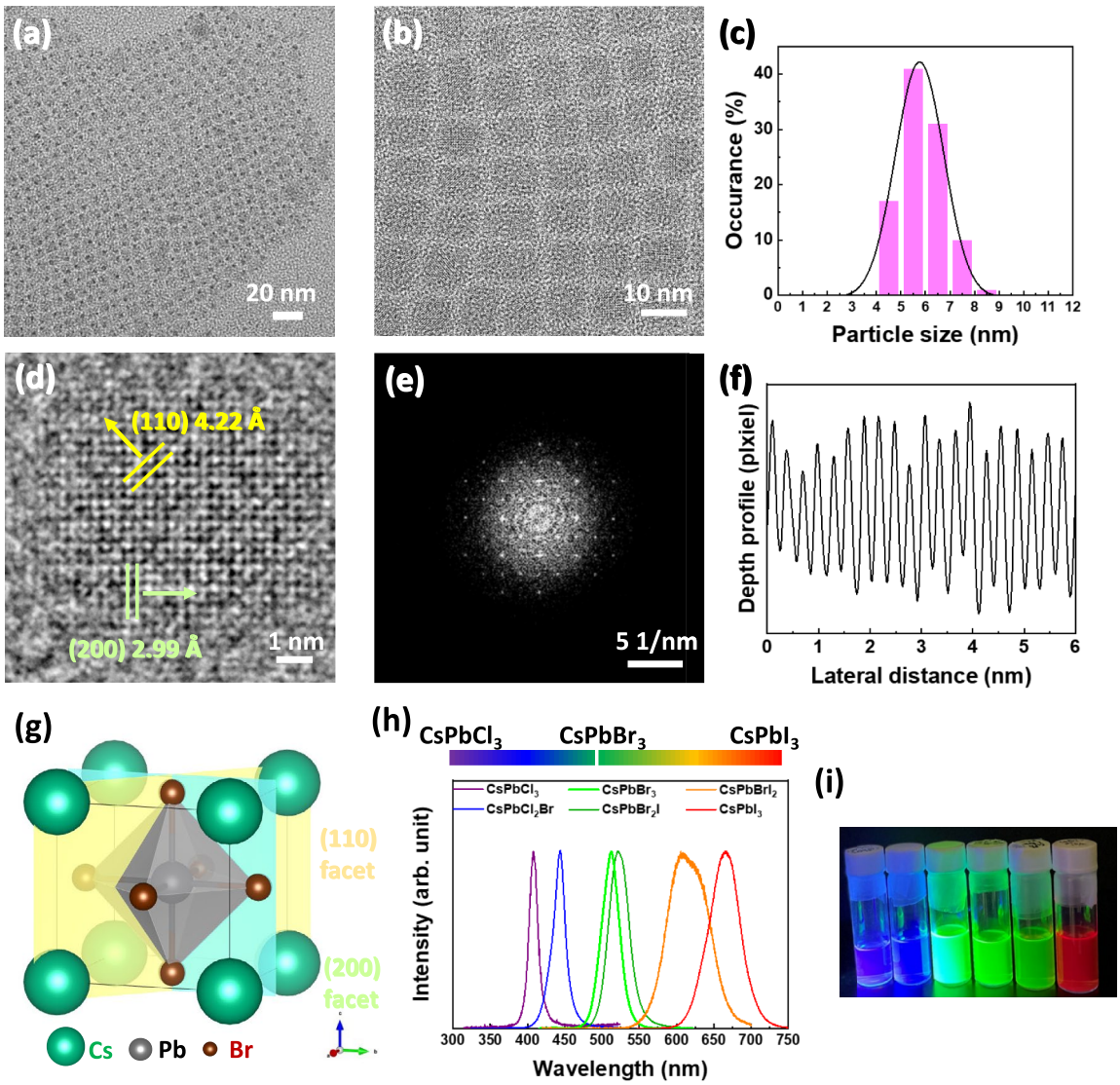

Fig. 1 Characteristic of as-synthesized quantum dots: **a** TEM image, **b** high-resolution TEM images, **c** statistic particle size distribution, **d** high-resolution TEM image for $d_{spacing}$ and plane observation, **e** diffraction pattern, **f** the depth profile for $d_{spacing}$ calculation, and **g** crystal structure of $CsPbBr_3$. **h** PL spectra, and **i** photos of various QDs solutions

are invaluable for tailoring the synthesis and application of QDs in advanced nanotechnology applications, paving the way for novel devices with enhanced performance and efficiency.

3.2 Phenomena of QD-embedded matrices

In a shared solvent system, QDs can be effectively dispersed and homogeneously mixed with polymers in a non-polar solvent, such as chlorobenzene. This enables the successful embedding of QDs into PMMA films with minimal aggregation. Unlike the amorphous polymer PMMA, P3HT is a semi-crystalline polymer, resulting in films containing both crystalline and amorphous phases. The crystallinity of P3HT influences the carrier mobility and conductivity of the film. For QD-embedded PMMA matrices, photoluminescence (PL) solely originates from the embedded QDs. The PL intensity increases as QD concentration rises, and PL emission peaks shift according to QD concentration in the QD-PMMA matrices. At low concentrations, embedded QDs are isolated by the insulating PMMA polymer matrix, resulting in a pronounced quantum confinement effect. This effect manifests as a noticeable blue shift in the 1.00 wt% QD-PMMA matrix compared to the 10.00 wt% QD-PMMA matrix, as shown in Fig. 2a. In contrast, the PL emission of QD-P3HT matrices behaves differently than that

of QD-PMMA matrices. QD exhibits minor PL emission when the concentration is below 10.00 wt%, as shown in Fig. 2b. Comparing QD-PMMA and QD-P3HT matrices, PL intensity from QDs in PMMA is strongly proportional to the numbers of QD in such matrices, as depicted in Fig. 2c. For QD-P3HT matrices, however, PL intensity evolves rapidly between 1.00 wt% and 10.00 wt%, as shown in Fig. 2d. This can be attributed to the carrier transfer between QD and P3HT matrices, which reduces the recombination of excited electron–hole pairs and energy release through photons in QD. In PMMA matrices, radiative recombination of QDs prevails over electron–hole pair transfer, leading to a linear relationship between PL intensity and QD concentration. When examining the carrier lifetime of QDs in both polymer matrices, the lifetime gradually approaches the pristine QD lifetime of 1.35 ns. The extended lifetime at low concentrations stems from the isolation effect of QD, while the reduced lifetime at high QD concentrations is due to QD aggregation in the PMMA matrix, as shown in Fig. 2e. Though P3HT matrices display a different lifetime trend in Fig. 2f, the lifetimes still approach the pristine QD value of 1.35 ns at a 10.00 wt% concentration. The well-dispersed distribution of QDs in P3HT matrices facilitates electron–hole pair transfer, resulting in a shorter QD lifetime.

To gain deeper insight into the effects of QD concentration, a series of QD-polymer matrices with concentrations ranging from 1.00 wt% to 5.00 wt% were prepared to observe the behavioral differences between insulating and conductive matrices, as shown in Fig. 3. Consistent with Fig. 2c, the emission peak of QD shifts noticeably with changes in concentration. As the QD concentration in PMMA increases, the blue shift of the emission peak disappears and returns to the wavelength emitted by the QD, around $\lambda = 505$ nm, as illustrated in Fig. 3a. A high concentration of QD in the matrix results in a dense QD distribution. The dense QD distribution causes the

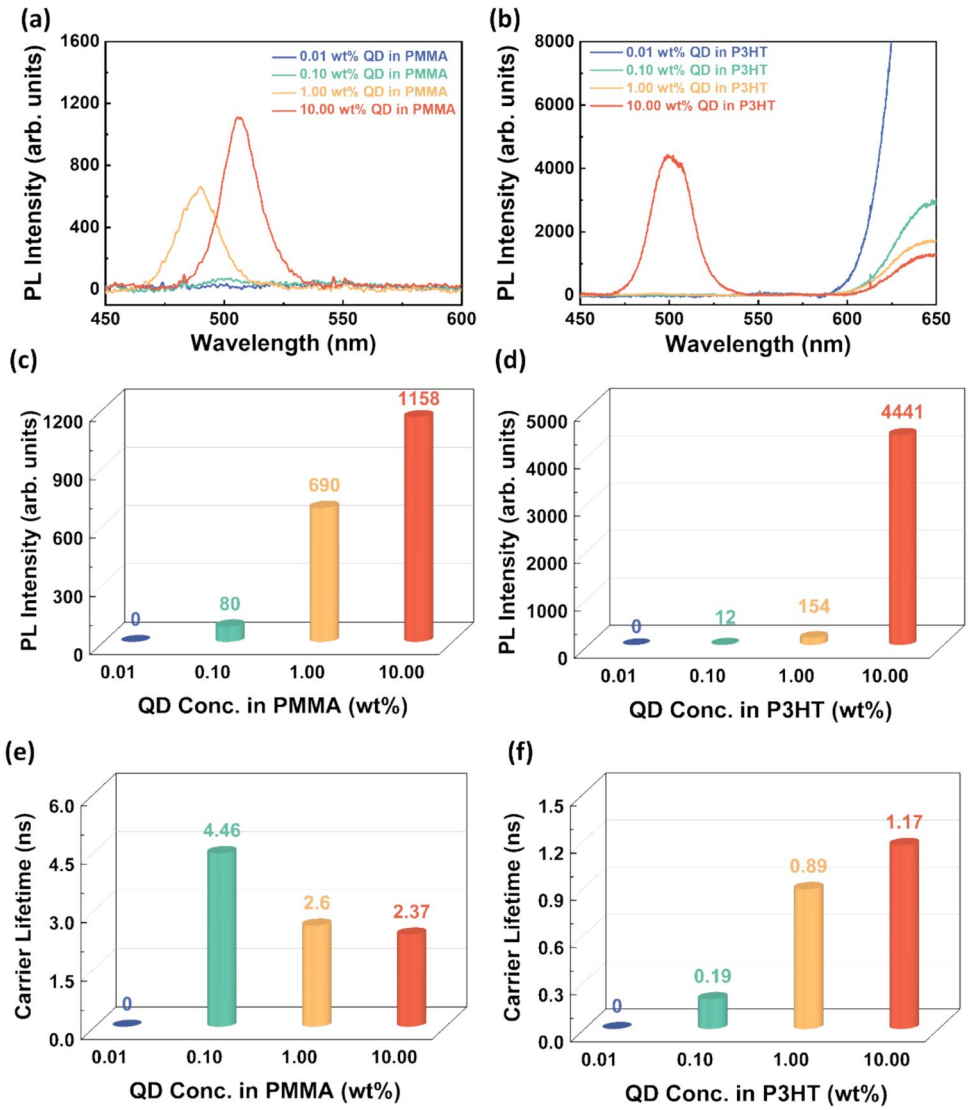

Fig. 2 $CsPbBr_3$ QD-embedded insulator (PMMA) and semiconductor (P3HT) polymer matrices: **a** PL spectra of QD-PMMA matrices, **b** PL spectra of QD-P3HT matrices, **c** PL intensity of QD-PMMA matrices, **d** PL intensity of QD-P3HT matrices, **e** carrier lifetime of QD-PMMA matrices, and **f** carrier lifetime of QD-P3HT matrices

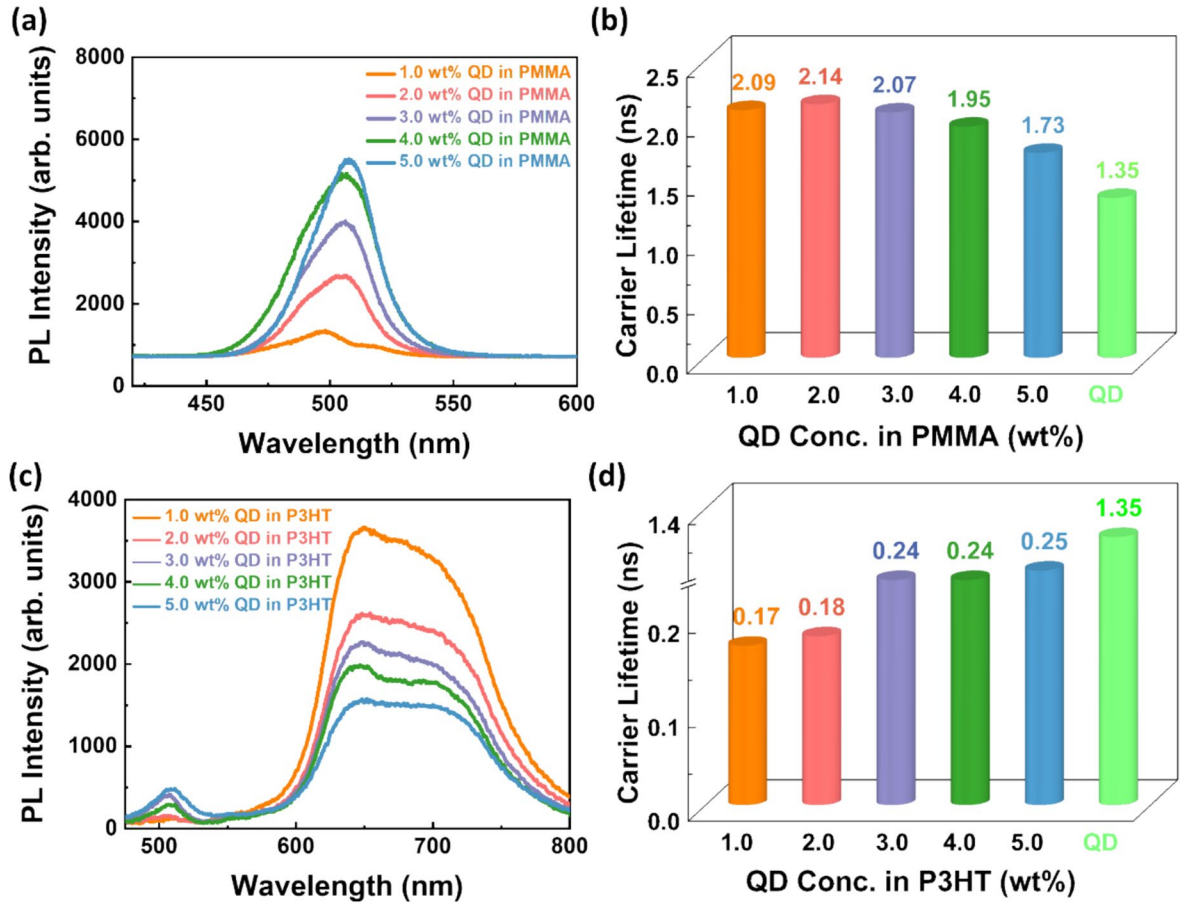

Fig. 3 Photoluminescence spectra and carrier lifetime of $CsPbBr_3$ quantum dot (QD) in an insulator or a conductive matrix: **a** PL spectra and **b** carrier lifetime of QD-PMMA matrices; **c** PL spectra and **d** carrier lifetime of QD-P3HT matrices

subtle isolation effect to produce a minor bandgap enlargement, resulting in a similar photoluminescence emission as the pristine QD at 505 nm. The PL intensity change is expected to be proportional to the QD concentration embedded in PMMA matrices, gradually increasing as the QD concentration rises. The relationship between the embedding concentration of QD in PMMA matrices and their carrier lifetime is depicted in Fig. 3b. The carrier lifetime of QD-PMMA matrices is clearly correlated with both concentration and PL intensity. The greater the distance between QDs, the higher the probability of carrier recombination through a slow process due to the long distance between adjacent QDs.

In contrast, for QD in a conductive P3HT matrix, the situation differs from the previous results. In Fig. 3c, the PL intensity of P3HT is significantly quenched when a small amount of QD is embedded into the P3HT matrices. The potential carrier transfer between P3HT and QD prevents the electron–hole pairs from recombining in the QD through a radiative pathway. When the QD concentration exceeds 2.00 wt%, the PL emission from QD becomes pronounced and exhibits a rapid increase. The carrier lifetime of these matrices is presented in Fig. 3d. The carrier lifetime deviates from the low concentration condition when the concentration surpasses 3.00 wt% (QD > 3.00 wt%). The carrier lifetime is markedly extended by around 40% compared to carriers in low concentration P3HT matrices (QD < 3.00 wt%).

To elucidate the behavior of carriers in matrices made of PMMA or P3HT, the binding energy (E_b) of quantum dots (QDs) was examined using temperature-dependent photoluminescent spectroscopy (Temp-PL). The Temp-PL measurements are presented in Figure S1 and S2. The exciton binding energy was estimated from Temp-PL results and calculated by Arrhenius equation [60]:

$$I(T) = \frac{I_0}{1 + Ae^{-\frac{E_b}{k_B T}}} \quad (1)$$

where $I(T)$ and I_0 are the integrated PL intensities at temperature T and 0 K; A is the ratio of the radiative to non-radiative times; E_b is the exciton binding energy, and k_B is the Boltzmann constant. As QDs tend to recombine through

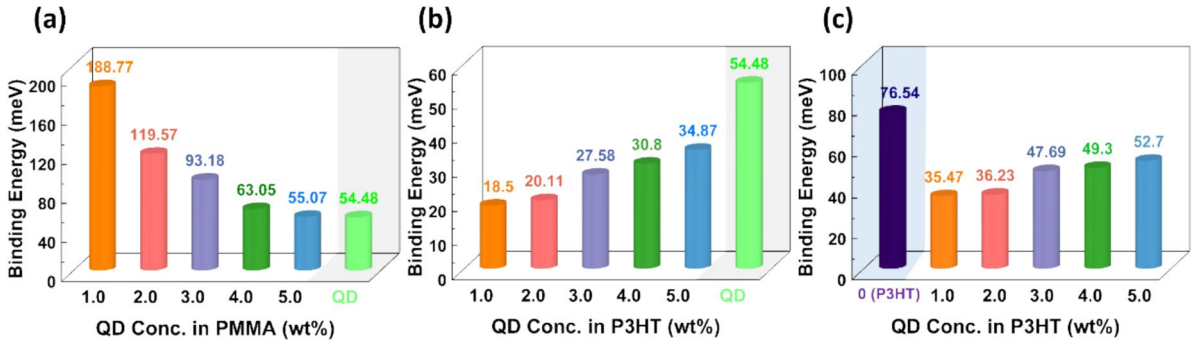

Fig. 4 Binding energy (E_b) evolution of QD in polymer matrices: **a** E_b of QD in PMMA matrices, **b** E_b of QD in P3HT matrices, and **c** E_b of P3HT matrices

Table 1 Binding energy of QD in different polymer matrices

QD concentration (wt%)	E_b of QD in a QD-PMMA matrix (meV)	E_b of QD in a QD-P3HT matrix (meV)	E_b of pristine QD (meV)
100.00	-	-	54.48
1.00	188.77	18.50	-
2.00	119.57	20.11	-
3.00	93.18	27.58	-
4.00	63.05	30.80	-
5.00	55.07	34.87	-

Table 2 Calculated binding energy of P3HT with QD embedding

QD concentration (wt%)	E_b of P3HT with QD embedding (meV)
0.00	76.54
1.00	35.47
2.00	36.23
3.00	47.69
4.00	49.30
5.00	52.70

radiative routes, they exhibit a higher E_b than three-dimensional perovskite materials with identical chemical composition. The calculated E_b values are shown in Fig. 4. The E_b of QDs in PMMA matrices decreases with increasing QD concentration. This can be attributed to the isolation effect of QDs in insulated PMMA matrices, where the carriers are confined and undergo radiative recombination. On the other hand, highly concentrated QD matrices exhibit behavior similar to pristine QD films, resulting in an E_b value similar to the intrinsic value of QD, as reported in Table 1.

Similarly, the E_b values of QDs in P3HT matrices provide insights into the energy required to separate excited electron–hole pairs to free carriers. The series of QD binding energy in P3HT matrices were studied using Temp-PL equipped with 405-nm and 532-nm pulse lasers, as illustrated in Figure S2 and S3. When the QDs concentration is low, the homogenous mixing of QDs with conductive P3HT reduce the E_b of QDs, indicating effective separation of excited electron–hole pairs. Conversely, as QD concentration exceeds 3.00 wt%, the E_b of QDs in P3HT matrices increases by 40% compared to low concentrations, approaching the E_b of pristine QD. This suggests that the interaction between conductive matrices and QD became less significant, and high QD concentrations in such matrices tend to aggregate, mimicking the behavior of pristine QD.

Furthermore, Fig. 4c and Table 2 presented the E_b values of P3HT matrices acquired from Temp-PL. For a pristine P3HT matrix, the E_b value was calculated to be 76.54 meV. As the QD concentration decreases below 3.00 wt%, the E_b value of P3HT matrices dramatically drop. Surprisingly, a sudden increase in E_b occurs between 2.00 and 3.00 wt% QD concentration, followed by a plateau region as QD concentration further increases.

3.3 Constructed field theory and mathematical calculation

The proposed carrier mechanism in these matrices is illustrated in Fig. 5. For QD-PMMA matrices (Fig. 5a), the dispersity of QD in PMMA matrices influences the carrier behavior. At low concentrations, the QDs are isolated and exhibit a significant energy level expansion due to quantum confinement. In contrast, at high concentrations, QD aggregation leads to bulk properties and a decrease in energy bandgap due to minor energy level discrete, as depicted in Fig. 5b. Focusing on conductive P3HT matrices, QDs are confined within and surrounded by the amorphous regions of semi-crystalline P3HT matrices, as shown in Fig. 5d. The close contact between QDs and amorphous P3HT enables efficient charge carrier transfer from QDs to P3HT matrices through the potential

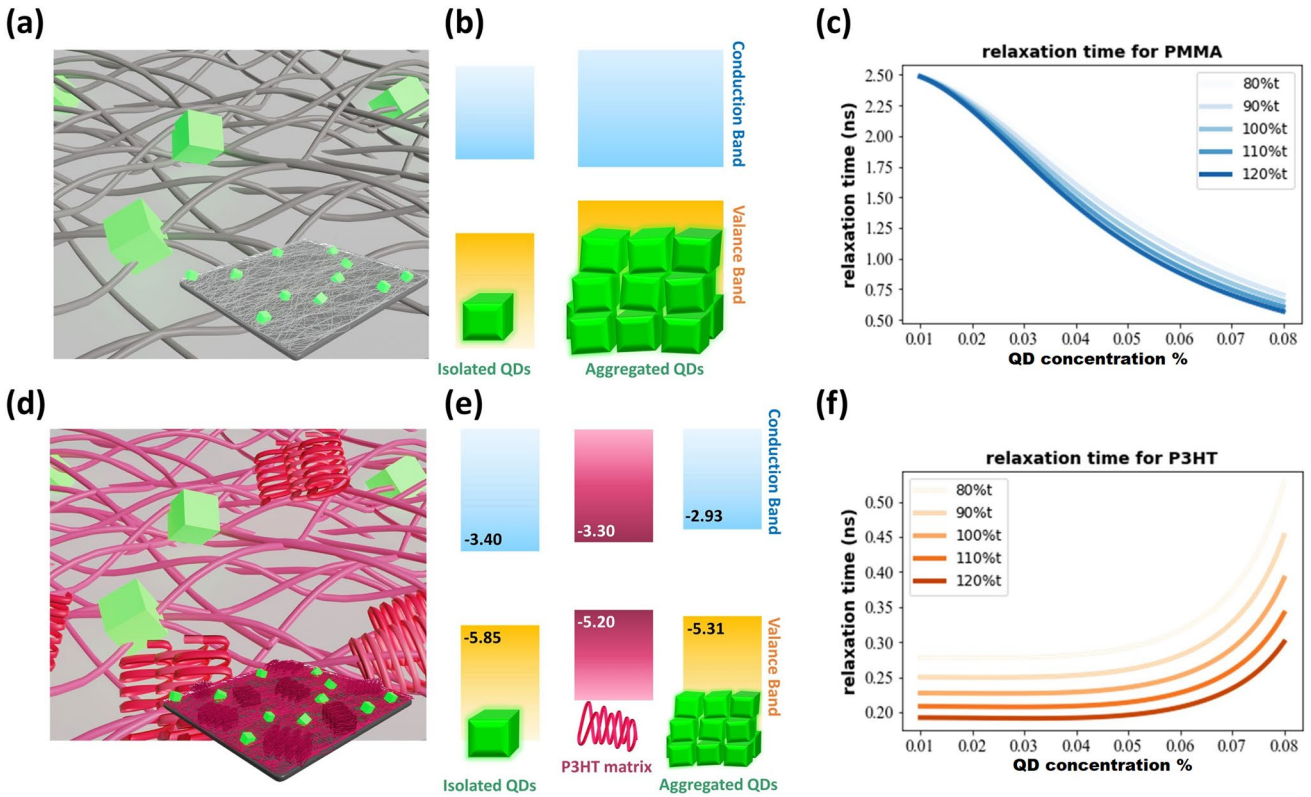

Fig. 5 Proposed scenarios QD in polymer matrices: **a** illustration, **b** proposed mechanism, and **c** calculated relaxation time of QD-PMMA matrix; **d** illustration, **e** proposed mechanism, and **f** calculated relaxation time of QD-P3HT matrix [55–57]. The calculated relaxation time for **c** PMMA and **f** P3HT is based on several assumptions and simplifications. The change of the relaxation time with respect to the QD concentration matches the experimental observations at least qualitatively which indicates the importance of the embedded QD's interactions with the different conduction matrix. The *t* represents the averaged transition amplitude, while the curves reveals that the increase of transition amplitude will reduce the relaxation time in varying degrees

difference at the interface (Fig. 5e). The high carrier density and suitable built-in potential (E_{bi}) at the interface might be the reason for the decreased E_b of carriers in P3HT matrices at embedded concentrations below 3.00 wt%. Due to the ease of carrier transfer from QDs to P3HT, the E_b of QDs in P3HT matrices also exhibits a relatively low value (Table 1). However, a high QD concentration in P3HT matrices may result in aggregation or even phase separation, rather than a uniform dispersion within the amorphous P3HT matrices. This hinders effective carrier transfer from QDs to P3HT matrices, causing both materials to exhibit their intrinsic properties with minimal interaction or interference between them.

To realize the scenario of QDs in semiconductor matrices from quantum physics point of view, we provide a self-contained theoretical framework to describe the phenomena of embedded QDs into the matrix solid. The non-interacting action of the matrix solid S_0 can be written as

$$S_0\left[\bar{\psi},\overline{\psi}\right]=\sum\nolimits_{kn\sigma}\left(-ik_n+\left(\varepsilon_{k\sigma}-\mu\right)\right)\overline{\psi}_{nk\sigma}\psi_{nk\sigma} \tag{2}$$

where $k_n=(2\pi+1)nk_BT$ is the Fermionic Matsubara frequency, and the summation over n is over Matsubara frequency, σ is the spin/band index, and $\overline{\psi}nk\sigma$ and ψnkσ are the field operators [61, 62]. Similarly, for a bunch of QDs $j,j=1,2,...,N_D$ centered at the locations $\boldsymbol{R}_j$ and energy levels $E_{\alpha\sigma}$, the QD action S_D can be written as

$$S_D\left[\bar{d},d\right]=\sum\nolimits_{jna\sigma}\left(-ik_n+E_{a\sigma}\right)\bar{d}_{na\sigma}\left(R_j\right)d_{nao}\left(R_j\right) \tag{3}$$

where $\bar{d}na\sigma(R)$ and $d_{na\sigma}(Rj)$ are the fields representing the QDs. Then, we consider the interaction term between QDs and matrix solid

$$S_T\left[\bar{d},d,\overline{\psi},\psi\right]=\sum\nolimits_{knja\sigma}\left[t_{ka\sigma}\left(R_j\right)\overline{\psi}_{nk\sigma}d_{na\sigma}\left(R_j\right)+t^*_{ka\sigma}\left(R_j\right)\bar{d}_{na\sigma}\left(R_j\right)\psi_{nk\sigma}\right] \tag{4}$$

where $t_{k\alpha\sigma}(\boldsymbol{R}_j)$ is the transition amplitude between the matrix electron with momentum **k** to the QD located at position $\boldsymbol{R}_j$. Performing explicit functional integral calculation, we have the effective action written as

$$S_{\text{eff}}[\overline{\psi},\psi] = S_0[\overline{\psi},\psi] + S_1[\overline{\psi},\psi]$$
$$S_1[\overline{\psi},\psi] = \frac{1}{L^d}\sum_{kqn\sigma} V_{kqn\sigma}\overline{\psi}_{nk+q\sigma}\psi_{nk\sigma} \quad (5)$$

where the scattering term $S_1[\overline{\psi},\overline{\psi}]$that contains the crucial observed new physics $V_{\boldsymbol{kq}n\sigma} = -L^d\sum_{j\alpha}\frac{E_{\alpha\sigma}}{E_{\alpha\sigma}^2+k_n^2}\left(t^*_{\boldsymbol{k}\alpha\sigma}(\boldsymbol{R}_j)t_{\boldsymbol{k}+\boldsymbol{q}\alpha\sigma}(\boldsymbol{R}_j)\right)$. With the help of self-averaging under the effective field similar to the impurity averaging, we construct the QD-averaged Green's function to study the transport properties [62, 63].

Taking $\boldsymbol{q}\to 0$. The second-order Green's function $G_\sigma^{(2)}(\boldsymbol{k},\boldsymbol{k}',ik_n)$ can be writtne as

$$\overline{G^{(2)}(\boldsymbol{k},\boldsymbol{k}',ik_n)} = G_\sigma^0(\boldsymbol{k},ik_n)\sum_{\boldsymbol{k}''}G_\sigma^0(\boldsymbol{k}'',ik_n)\overline{V_{\boldsymbol{k}\boldsymbol{k}''n\sigma}V_{\boldsymbol{k}''\boldsymbol{k}'n\sigma}}G_\sigma^0(\boldsymbol{k}',ik_n) \quad (6)$$

where $G_\sigma^0(\boldsymbol{k},ik_n)$ is the free-electron Green's function for matrix solid only, $\overline{V_{\boldsymbol{k}\boldsymbol{k}''n\sigma}V_{\boldsymbol{k}''\boldsymbol{k}'n\sigma}}$ means the connected part of scattering with respect to QDs averaging with normal distribution. The QDs' distribution satisfied the normal distribution with average $t_{0\boldsymbol{k}\alpha\sigma}$ and covarience matrix $\Sigma_{\boldsymbol{k}\alpha\sigma}$. After some math, we have the self energy

$$\Sigma(k,ik_n)\ amp; = \sum_{k''}G_\sigma^0(k'',ik_n)\overline{V_{kk''n\sigma}V_{k'k''n\sigma}}$$
$$amp; = \sum_{k''}\frac{1}{ik_n-\epsilon_{k''}+\mu}\overline{V_{kk''n\sigma}V_{k'k''n\sigma}} \quad (7)$$

where $\overline{V_{\boldsymbol{k}\boldsymbol{k}''n\sigma}V_{\boldsymbol{k}''\boldsymbol{k}'n\sigma}} = N_D\delta_{\boldsymbol{k}\boldsymbol{k}'}\sum_{\alpha\alpha'}\frac{t_{0\boldsymbol{k}\alpha\sigma}t^*_{0\boldsymbol{k}\alpha'\sigma}+\delta_{\alpha\alpha'}\Sigma^2_{\boldsymbol{k}\alpha\sigma}}{ik_n-E_\alpha}\sum_{\boldsymbol{k}_1}\frac{t_{0\boldsymbol{k}_1\alpha\sigma}t^*_{0\boldsymbol{k}_1\alpha'\sigma}+\delta_{\alpha\alpha'}\Sigma^2_{\boldsymbol{k}_1\alpha\sigma}}{ik_n-E_{\alpha'}}$
$+N_D(N_D-1)\delta_{\boldsymbol{k},\boldsymbol{k}_1}\delta_{\boldsymbol{k}_1\boldsymbol{k}'}\sum_{\alpha\alpha'}\frac{\left|t_{0\boldsymbol{k}\alpha\sigma}\right|^2+\Sigma^2_{\boldsymbol{k}\alpha\sigma}}{ik_n-E_\alpha}\frac{\left|t_{0\boldsymbol{k}'\alpha'\sigma}\right|^2+\Sigma^2_{\boldsymbol{k}'\alpha'\sigma}}{ik_n-E_{\alpha'}}$.

This can fully describe the effect of different QD concentration embedded semiconductor matrices of P3HT and insulator matrices of PMMA. The explicit expression of the self-energy implies the important role of the QD's energy levels, which appear in the denominator. With the help of some assumptions and simplifications, the calculated relaxation time is presented in Fig. 5c and 5h. We can see the relaxation time of the carrier for P3HT increase with the QD concentration while the relaxation time for PMMA would decrease with the increasing QD concentration. This result at least qualitatively matches what we observed from the experiments. Detailed derivation and the explanation should refer to the supplementary information.

4 Conclusion

This study explores the utilization of constructive quantum field theory to explain the non-perturbative behavior of quantum dot (QD)-embedded matrices in different solid-state systems. Conducting P3HT matrices can mediate a non-perturbative QD interactions that lead to qualitatively distinct properties, including the enhanced carrier lifetime and enhanced binding energies. The remarkable changes of both properties can be observed within the QD concentration range of 2.00 to 3.00 wt.%. In a sharp contrast, the binding energy and carrier lifetime observed in QD-embedded PMMA matrices are highly dependent on QD-embedded concentration. The proposed new principle, derived from the second-order expansion of the QD-averaged Green's function, leverages matrix-mediated QD interactions to tailor the light-matter interaction within the matrices. It turns the table on the lack of clear underlying designing principles and alleviates heavily reliant on trial-and-error methods. The phenomena, which cannot be explained by conventional perturbative scattering theories, demonstrate qualitative agreement with experimental observations. The effective theory constructs a simplified yet robust framework to provide the generalized and fundamental insights into the physics systems, with only a large bulk matrix, the randomly dispersed quantum dots, and their interactions. It relies on certain assumptions, such as treating the matrix as a weakly correlated Fermi system and considering the quantum dots to be randomly distributed with discrete energy levels due to their small size. Despite these assumptions, the theory demonstrates remarkable generality and provides deep insights through indicating the possible interacting mechanism between bulk matrices and dispersed quantum dots observed through experiments. This makes it a powerful tool for exploring a wide range of materials properly under the effective field framework such as carrier transport and perhaps electron–phonon coupling, magnetism in the future. Overall, this work provides a foundation for the predictive design of advanced hybrid materials, aiming to optimize their functionalities. The findings contribute to the field's understanding of quantum dot-embedded matrices and pave the way for future investigations into the underlying principles and potential applications of such systems.

Supplementary Information The online version contains supplementary material available at https://doi.org/10.1007/s42114-025-01358-2.

Acknowledgements The authors appreciate Dr. Ming-Tao Lee (BL-13A1), Dr. Jeng-Lung Chen (BL-17C1), and Dr. Ting-Shan Chan (BL-01C1) and Dr. Chia-Hsin Wang (BL-24A1) at National Synchrotron Radiation Research Centre for helpful discussion and suggestions, and Mr. Y.-S. Chen at Instrumentation Centre of National Tsing Hua University for TEM analysis. The authors thank the Microscopy Center at Chang Gung University for technical assistance.

Author contribution M.-C. W, M. L., M.-P. N., Y.-C. H., and W.-F. S. conceived and designed this work. K.-C. H, T.-H. L., and Y.-H. C. fabricated the samples, tested the properties, and processed the related data. C. F. performed the theory calculations. The manuscript was drafted by K.-C. H and C. F. and revised by M.-C. W and M. L.. All authors provided critical feedback and helped shape the research, analysis and manuscript.

Funding The financial support from the National Science and Technology Council, Taiwan (Project No. 111–2221-E-182 -040 -MY3, and 113–2628-E-182–001-MY4, and 114–2923-E-182–001-MY3), and Chang Gung Memorial Hospital at Linkou (CMRPD2N0062 and BMRPC74) are highly appreciated. The author expresses

gratitude for the financial support provided by Chang Gung University (URRPD2Q0021, URRPD2Q0031, and URRPD2Q0041).

Data availability No datasets were generated or analysed during the current study.

Declarations

Conflict of interest The authors declare no competing interests.

Open Access This article is licensed under a Creative Commons Attribution 4.0 International License, which permits use, sharing, adaptation, distribution and reproduction in any medium or format, as long as you give appropriate credit to the original author(s) and the source, provide a link to the Creative Commons licence, and indicate if changes were made. The images or other third party material in this article are included in the article's Creative Commons licence, unless indicated otherwise in a credit line to the material. If material is not included in the article's Creative Commons licence and your intended use is not permitted by statutory regulation or exceeds the permitted use, you will need to obtain permission directly from the copyright holder. To view a copy of this licence, visit http://creativecommons.org/licenses/by/4.0/.

References

1. Doering WE, Nie S (2003) Spectroscopic TaGs using dye-embedded nanoparticles and surface-enhanced Raman scattering. Anal Chem 75:6171–6176. https://doi.org/10.1021/ac034672u
2. Arici E, Sariciftci NS, Meissner D (2003) Hybrid solar cells based on nanoparticles of $CuInS_2$ in organic matrices. Adv Func Mater 13:165–171. https://doi.org/10.1002/adfm.200390024
3. Kirkengen M, Bergli J, Galperin YM (2007) Direct generation of charge carriers in C-Si solar cells due to embedded nanoparticles. J Appl Phys 102:093713. https://doi.org/10.1063/1.2809368
4. Lu L, Luo Z, Xu T, Yu L (2013) Cooperative plasmonic effect of Ag and Au nanoparticles on enhancing performance of polymer solar cells. Nano Letter 13:59–64. https://doi.org/10.1021/nl3034398
5. Awazu K, Fujimaki M, Rockstuhl C, Tominaga J, Murakami H, Ohki Y, Yoshida N, Watanabe T (2008) A plasmonic photocatalyst consisting of silver nanoparticles embedded in titanium dioxide. J Am Chem Soc 130:1676–1680. https://doi.org/10.1021/ja076503n
6. Kim K-K, Koguchi N, Ok Y-W, Seong T-Y, Park S-J (2004) Fabrication of ZnO quantum dots embedded in an amorphous oxide layer. Appl Phys Lett 84:3810–3812. https://doi.org/10.1063/1.1741030
7. Landin L, Miller MS, Pistol ME, Pryor CE, Samuelson L (1998) Optical studies of individual inas quantum dots in gaas: few-particle effects. Science 280:262. https://doi.org/10.1126/science.280.5361.262
8. Mirabella S, Agosta R, Franzò G, Crupi I, Miritello M, Lo SR, Di Stefano MA, Di Marco S, Simone F, Terrasi A (2009) Light absorption in silicon quantum dots embedded in silica. J Appl Phys 106:103505. https://doi.org/10.1063/1.3259430
9. Rainò G, Becker MA, Bodnarchuk MI, Mahrt RF, Kovalenko MV, Stöferle T (2018) Superfluorescence from lead halide perovskite quantum dot superlattices. Nature. https://doi.org/10.1038/s41586-018-0683-0
10. Valerini D, Cretí A, Lomascolo M, Manna L, Cingolani R, Anni M (2005) Temperature dependence of the photoluminescence properties of colloidal CdSe/ZnS core/shell quantum dots embedded in a polystyrene matrix. Phys Rev B 71:235409
11. Yang P, Song CF, Lü MK, Yin X, Zhou GJ, Xu D, Rong YD (2001) The luminescence of PbS nanoparticles embedded in sol–gel silica glass. Chem Phys Lett 345:429–434. https://doi.org/10.1016/S0009-2614(01)00926-5
12. Jamet M, Dupuis V, Mélinon P, Guiraud G, Pérez A, Wernsdorfer W, Traverse A, Baguenard B (2000) Structure and magnetism of well defined cobalt nanoparticles embedded in a niobium matrix. Phys Rev B 62:493–499
13. Golosovsky IV, Mirebeau I, Andre G, Kurdyukov DA, Kumzerov YA, Vakhrushev SB (2001) Magnetic ordering and phase transition in MnO embedded in a porous glass. Phys Rev Lett 86:5783–5786. https://doi.org/10.1103/PhysRevLett.86.5783
14. Sort J, Langlais V, Doppiu S, Dieny B, Suriñach S, Muñoz JS, Baró MD, Ch L, Nogués J (2004) Exchange bias effects in Fe nanoparticles embedded in an antiferromagnetic Cr_2O_3 matrix. Nanotechnology 15:S211
15. Nogues J, Sort J, Langlais V, Doppiu S, Dieny B, Muñoz J, Suriñach S, Baró M, Sort J, Langlais V, Doppiu S, Dieny B, Muñoz J, Suriñach S, Baró M (2005) Exchange bias in ferromagnetic nanoparticles embedded in an antiferromagnetic matrix. Int J Nanotechnol 2:24. https://doi.org/10.1002/chin.200602225
16. Fonseca FC, Goya GF, Jardim RF, Muccillo R, Carreño NLV, Longo E, Leite ER (2002) Superparamagnetism and magnetic properties of Ni nanoparticles embedded in SiO_2. Phys Rev B 66:104406
17. Koblischka-Veneva A, Koblischka MR, Babu NH, Cardwell DA, Shlyk L, Krabbes G (2006) An electron backscatter diffraction investigation of crystallographic orientations of embedded nanoparticles within melt-textured YbCo high temperature superconductors. Supercond Sci Technol 19:S562–S566. https://doi.org/10.1088/0953-2048/19/7/s27
18. Snezhko A, Prozorov T, Prozorov R (2005) Magnetic nanoparticles as efficient bulk pinning centers in type-II superconductors. Phys Rev B 71:024527. https://doi.org/10.1103/PhysRevB.71.024527
19. Guimarães ÉV, Vasconcelos CAA, Silva RS, Cano NF, Dantas NO (2023) Evidence of formation of diluted magnetic semiconductor $Sn_{1-x}Mn_xTe$ quantum dots in glass matrix. Physica B 666:415089. https://doi.org/10.1016/j.physb.2023.415089
20. Kim W, Zide J, Gossard A, Klenov D, Stemmer S, Shakouri A, Majumdar A (2006) Thermal conductivity reduction and thermoelectric figure of merit increase by embedding nanoparticles in crystalline semiconductors. Phys Rev Lett 96:045901. https://doi.org/10.1103/PhysRevLett.96.045901
21. Kundu A, Mingo N, Broido DA, Stewart DA (2011) Role of light and heavy embedded nanoparticles on the thermal conductivity of SiGe alloys. Phys Rev B 84:125426. https://doi.org/10.1103/PhysRevB.84.125426
22. Katcho NA, Mingo N, Broido DA (2012) Lattice thermal conductivity of $(Bi_{1-x}Sb_x)_2Te_3$ alloys with embedded nanoparticles. Phys Rev B 85:115208. https://doi.org/10.1103/PhysRevB.85.115208
23. Ma Y, Heijl R, Palmqvist AEC (2012) Composite thermoelectric materials with embedded nanoparticles. J Mater Sci 48:2767–2778. https://doi.org/10.1007/s10853-012-6976-z
24. Zhao L-D, Dravid VP, Kanatzidis MG (2014) The panoscopic approach to high performance thermoelectrics. Energy Environ Sci 7:251–268. https://doi.org/10.1039/c3ee43099e
25. García de Arquer F. P., Gong X., Sabatini R. P., Liu M., Kim G.-H., Sutherland B. R., Voznyy O., Xu J., Pang Y., Hoogland S., Sinton D., Sargent E. (**2017**) Field-emission from quantum-dot-in-perovskite solids. *Nature Communications*, 8: 14757. https://doi.org/10.1038/ncomms14757 https://www.nature.com/articles/ncomms14757#supplementary-information

26. Li G-S, Zhang D-Q, Yu JC (2009) A new visible-light photocatalyst: CdS quantum dots embedded mesoporous TiO_2. Environ Sci Technol 43:7079–7085. https://doi.org/10.1021/es9011993
27. Ning Z, Gong X, Comin R, Walters G, Fan F, Voznyy O, Yassitepe E, Buin A, Hoogland S, Sargent EH (2015) Quantum-dot-in-perovskite solids. Nature 523:324–328. https://doi.org/10.1038/nature14563
28. Meinardi F, Colombo A, Velizhanin KA, Simonutti R, Lorenzon M, Beverina L, Viswanatha R, Klimov VI, Brovelli S (2014) Large-area luminescent solar concentrators based on 'stokes-shift-engineered' nanocrystals in a mass-polymerized pmma matrix. Nat Photonics 8:392–399. https://doi.org/10.1038/nphoton.2014.54
29. Tu Z, Yang G, Song H, Wang C (2017) Amorphous ZnO quantum dot/mesoporous carbon bubble composites for a high-performance lithium-ion battery anode. ACS Appl Mater Interfaces 9:439–446. https://doi.org/10.1021/acsami.6b13113
30. Arvand M, Hemmati S (2017) Magnetic nanoparticles embedded with graphene quantum dots and multiwalled carbon nanotubes as a sensing platform for electrochemical detection of progesterone. Sens Actuators, B Chem 238:346–356. https://doi.org/10.1016/j.snb.2016.07.066
31. Nath SS, Choudhury M, Chakdar D, Gope G, Nath RK (2010) Acetone sensing property of ZnO quantum dots embedded on PVP. Sens Actuators, B Chem 148:353–357. https://doi.org/10.1016/j.snb.2010.06.001
32. Sathe TR, Agrawal A, Nie SM (2006) Mesoporous silica beads embedded with semiconductor quantum dots and iron oxide nanocrystals: dual-function microcarriers for optical encoding and magnetic separation. Anal Chem 78:5627–5632. https://doi.org/10.1021/ac0610309
33. Beier HT, Cote GL, Meissner KE (2009) Whispering gallery mode biosensors consisting of quantum dot-embedded microspheres. Ann Biomed Eng 37:1974–1983. https://doi.org/10.1007/s10439-009-9713-2
34. Pang S, Beckham RE, Meissner KE (2008) Quantum dot-embedded microspheres for remote refractive index sensing. Appl Phys Lett 92:221108–2211083. https://doi.org/10.1063/1.2937209
35. Li H, Li Y, Cheng J (2010) Molecularly imprinted silica nanospheres embedded CdSe quantum dots for highly selective and sensitive optosensing of pyrethroids. Chem Mater 22:2451–2457. https://doi.org/10.1021/cm902856y
36. Vineis CJ, Shakouri A, Majumdar A, Kanatzidis MG (2010) Nanostructured thermoelectrics: big efficiency gains from small features. Adv Mater 22:3970–3980. https://doi.org/10.1002/adma.201000839
37. Zhao W, Liu Z, Sun Z, Zhang Q, Wei P, Mu X, Zhou H, Li C, Ma S, He D, Ji P, Zhu W, Nie X, Su X, Tang X, Shen B, Dong X, Yang J, Liu Y, Shi J (2017) Superparamagnetic enhancement of thermoelectric performance. Nature 549:247–251. https://doi.org/10.1038/nature23667
38. García de Arquer FP, Talapin DV, Klimov VI, Arakawa Y, Bayer M, Sargent EH. Semiconductor quantum dots: Technological progress and future challenges. Science. 2021 373(6555):eaaz8541. https://doi.org/10.1126/science.aaz8541
39. Lu W-G, Wu X-G, Huang S, Wang L, Zhou Q, Zou B, Zhong H, Wang Y (2017) Strong polarized photoluminescence from stretched perovskite-nanocrystal-embedded polymer composite films. Adv Opt Mater 5:1700594. https://doi.org/10.1002/adom.201700594
40. Tselikov GI, Timoshenko VY, Golovan LA, Plenge J, Shatalova AM, Shandryuk GA, Kutergina IY, Merekalov AS, Rühl E, Talroze RV (2015) Role of the polymer matrix on the photoluminescence of embedded CdSe quantum dots. ChemPhysChem 16:1071–1078. https://doi.org/10.1002/cphc.201402913
41. Gu X, Huang Z, Xu W, Gao S, Zhang H, Tao X, Zhao Y, Huang S (2024) Enhanced stability of perovskite CsPbBr3 QDs via synergetic encapsulation with zno nanocrystals and commercial polymer. J Lumin 275:120780. https://doi.org/10.1016/j.jlumin.2024.120780
42. Xu Y, Wang W, Chen Z, Sui X, Wang A, Liang C, Chang J, Ma Y, Song L, Jiang W, Zhou J, Liu X, Zhang Y (2021) A general strategy for semiconductor quantum dot production. Nanoscale 13:8004–8011. https://doi.org/10.1039/D0NR09067K
43. Xu M, Zhang W, Yang Z, Yu F, Ma Y, Hu N, He D, Liang Q, Su Y, Zhang Y (2015) One-pot liquid-phase exfoliation from graphite to graphene with carbon quantum dots. Nanoscale 7:10527–10534. https://doi.org/10.1039/C5NR02198G
44. Alivisatos AP (1996) Semiconductor clusters, nanocrystals, and quantum dots. Science 271:933–937. https://doi.org/10.1126/science.271.5251.933
45. Liu M, Yazdani N, Yarema M, Jansen M, Wood V, Sargent EH (2021) Colloidal quantum dot electronics. *Nature*. Electronics 4:548–558. https://doi.org/10.1038/s41928-021-00632-7
46. Bai Y, Hao M, Ding S, Chen P, Wang L (2022) Surface chemistry engineering of perovskite quantum dots: strategies, applications, and perspectives. Adv Mater 34:2105958. https://doi.org/10.1002/adma.202105958
47. Pan J, Shang Y, Yin J, De Bastiani M, Peng W, Dursun I, Sinatra L, El-Zohry AM, Hedhili MN, Emwas A-H, Mohammed OF, Ning Z, Bakr OM (2018) Bidentate ligand-passivated $CsPbI_3$ perovskite nanocrystals for stable near-unity photoluminescence quantum yield and efficient red light-emitting diodes. J Am Chem Soc 140:562–565. https://doi.org/10.1021/jacs.7b10647
48. Liu F, Zhang Y, Ding C, Kobayashi S, Izuishi T, Nakazawa N, Toyoda T, Ohta T, Hayase S, Minemoto T, Yoshino K, Dai S, Shen Q (2017) Highly luminescent phase-stable $CsPbI_3$ perovskite quantum dots achieving near 100% absolute photoluminescence quantum yield. ACS Nano 11:10373–10383. https://doi.org/10.1021/acsnano.7b05442
49. Shi W, Yao Q, Donghui W, Qu S, Chen Y, Lee KH, Chen L (2022) Vapor phase polymerization of Ag QD-embedded PEDOT film with enhanced thermoelectric and antibacterial properties. NPG Asia Materials 14:47. https://doi.org/10.1038/s41427-022-00391-7
50. Jena D, Gossard AC, Mishra UK (2000) Dislocation scattering in a two-dimensional electron gas. Appl Phys Lett 76:1707. https://doi.org/10.1063/1.126143
51. Dexter DL, Seitz F (1952) Effects of dislocations on mobilities in semiconductors. Phys Rev 86:964–965. https://doi.org/10.1103/PhysRev.86.964
52. Look DC, Sizelove JR (1999) Dislocation scattering in gan. Phys Rev Lett 82:1237–1240
53. Podor B (1966) Electron mobility in plastically deformed germanium. Phys Status Solidi 16:K167–K0. https://doi.org/10.1002/pssb.19660160264
54. Weimann NG, Eastman LF, Doppalapudi D, Ng HM, Moustakas TD (1998) Scattering of electrons at threading dislocations in GaN. J Appl Phys 83:3656–3659
55. Mayadas AF, Shatzkes M (1970) Electrical-resistivity model for polycrystalline films: the case of arbitrary reflection at external surfaces. Phys Rev B 1:1382–1389
56. Tellier CR (1978) A theoretical description of grain boundary electron scattering by an effective mean free path. Thin Solid Films 51:311–317. https://doi.org/10.1016/0040-6090(78)90293-6
57. Faleev SV, Léonard F (2008) Theory of enhancement of thermoelectric properties of materials with nanoinclusions. Phys Rev B 77:214304. https://doi.org/10.1103/PhysRevB.77.214304
58. Cronenwett SM, Oosterkamp TH, Kouwenhoven LP (1998) A tunable kondo effect in quantum dots. Science 281:540
59. Beenakker CWJ (1991) Theory of coulomb-blockade oscillations in the conductance of a quantum dot. Phys Rev B 44:1646–1656. https://doi.org/10.1103/PhysRevB.44.1646

60. Lee K-M, Chan S-H, Hou M-Y, Chu W-C, Chen S-H, Yu S-M, Wu M-C (2021) Enhanced efficiency and stability of quasi-2D/3D perovskite solar cells by thermal assisted blade coating method. Chem Eng J 405:126992. https://doi.org/10.1016/j.cej.2020.126992
61. Alexander Altland BDS. (2010) Condensed matter field theory. Cambridge University Press.
62. Coleman P (2015) Introduction to many-body physics. Cambridge University Press
63. Henrik Bruus KF. (2004) Many-body quantum theory in condensed matter physics: an introduction. Oxford University Press.

Publisher's Note Springer Nature remains neutral with regard to jurisdictional claims in published maps and institutional affiliations.